A simulation study of induced disorder, failure and fracture of perfect metal crystals under uniaxial tension

1995 J. Phys.: Condens. Matter 7 4603

(http://iopscience.iop.org/0953-8984/7/24/003)

J. Phys.: Condens. Matter 7 (1995) 4603–4624. Printed in the UK

A simulation study of induced disorder, failure and fracture of perfect metal crystals under uniaxial tension

R M Lynden-Bell
School of Mathematics and Physics, The Queen's University, Belfast BT7 1NN, UK

Received 24 January 1995, in final form 11 April 1995

Abstract. The behaviour of FCC crystals of the metals platinum, gold, rhodium and silver under uniaxial tension was investigated using atomistic simulation. At temperatures above half the melting temperature all the model metals disordered before they failed by void formation. Investigation of the free energy as a function of order parameter showed that this process occurs when the free energies of the ordered and disordered states are equal, rather than at the limit of metastability of the stretched crystal. At lower temperatures different behaviour was seen in different metals; in the more ductile metals local regions of disorder appear first, while in the other metals defects are generated by sliding of planes of atoms.

1. Introduction

The way in which perfect crystals fracture under different geometrical constraints is of considerable interest, and is a topic that can appropriately be investigated by atomistic computer simulation. Although the fracture of real crystals is usually determined by defects, the ultimate strength of materials depends on the way in which defect-free crystals break [1]. The most nearly perfect crystals known are whiskers. Rather analogous to these are the bridges formed in scanning tunnelling microscopy, when a tip touches a flat surface and is then withdrawn. Under some circumstances a thin whisker of material is pulled out [2, 3]. Agraït and co-workers [3] have shown that whiskers of lead formed in this way show a succession of steps in the stress–strain curves.

The principal factors affecting the way in which perfect crystals fracture are the type of material, the temperature and the constraints under which the material is stretched.

Numerical experiments using atomistic simulation have previously been used to investigate the failure of perfect crystals at finite temperatures. Parrinello and Rahman [4] were the first to show the effects of temperature on the failure of a perfect crystalline material. Wang and co-workers [5], Maguire [6] and more recently Blonski and co-workers [7] have investigated stress and fracture of two-dimensional systems at finite temperatures, while Lynden-Bell [8, 9] and Selinger and co-workers [10] have looked at three-dimensional systems of various types.

In this work samples of FCC metals are stretched along their (100) directions, with the lateral dimensions constrained to be constant. In the initial stages the material remains ordered, but at temperatures of approximately half the melting temperature or higher, disorder sets in as the stress reaches its maximum value. This is the point of failure and is quickly followed by void formation and fracture. At lower temperatures different behaviour is seen in different materials. In the more ductile platinum/gold model a local region of disorder forms, while in the model for rhodium/silver planes of atoms are seen

0953-8984/95/244603+22$19.50

to slip sideways relative to each other. The behaviour of platinum/gold can be interpreted in terms of the Landau free energy curves of the disordered and ordered materials. The differences between the two materials are discussed.

2. Methods

2.1. Potential

Numerical experiments were carried out on two different metals. In order to model metals in an atomistic simulation it is necessary to go beyond a simple pair potential. In this work we used the potentials of the Finnis–Sinclair type [11], as developed by Sutton and Chen [12]. In these potentials

$$V = \epsilon\left[\sum_{\text{pairs}}\left(\frac{a}{r_{ij}}\right)^n - c\sum_i \rho_i^{1/2}\right] \tag{1}$$

where ρ_i, the density at atom i, is modelled by

$$\rho_i = \sum_j \left(\frac{a}{r_{ij}}\right)^m. \tag{2}$$

Although this is truly a many-body potential, the force on each atom can be written as a sum of pairwise contributions

$$\boldsymbol{F}_i = \sum_j \boldsymbol{F}_{ij} \tag{3}$$

where

$$\boldsymbol{F}_{ij} = \epsilon\left[n\left(\frac{a}{r_{ij}}\right)^n - \tfrac{1}{2}Cm(\rho_i^{-1/2} + \rho_j^{-1/2})\left(\frac{a}{r_{ij}}\right)^m\right]\frac{\boldsymbol{r}_{ij}}{r_{ij}^2}. \tag{4}$$

These potentials contain two exponents, n and m, and two parameters, ϵ and a, which determine the scales for energy and distance respectively. It should be noted that c is not a free parameter but is determined by the requirement that a be equal to the equilibrium lattice constant at zero temperature. Metals modelled with different exponents have different properties, while the properties of metals modelled with the same exponents but different values of the scaling parameters are the same in terms of reduced units of ϵ for energy and a for distance.

Sutton and Chen [12] used bulk properties to assign exponents to different FCC metals. Their work, and subsequent investigations [13], have shown that the family of Sutton–Chen potentials of this type ranges from very ductile materials, in which n and m have similar values (for example platinum and gold with $n = 10, m = 8$) to less ductile materials, in which n and m differ more widely (for example silver and rhodium with $n = 12, m = 6$). The potential for platinum/gold is both softer and more short-ranged than that for rhodium/silver.

All the static properties of materials with the same values of m and n scale, so that if we do a calculation with, say, $n = 10, m = 8$ we can predict the behaviour of both platinum and gold. It should be noted that as these potentials have few parameters they cannot be

Table 1. Some properties of the materials used.

Metal	a_0^a [Å]	U_0 [10^3 K]	T_m [K]	kT_m [U_0]	ΔH_{fus} [U_0]	E_{surf} [$a_{nn}U_0$]	ΔV [V_0]	C_{11}^0/B	C_{12}^0/B	C_{44}^0/B
Pt (model)	3.92	67.84	1400 ± 50	0.021	0.025	8.4%	7.8%	1.13	0.93	0.27
Pt (expt.)			(2042)	(0.030)	(0.040)			(1.24)	(0.88)	(0.27)
Au (model)	4.08	43.76	880 ± 30	0.021	0.025	8.4%	7.8%	1.13	0.93	0.27
Au (expt.)			(1338)	(0.030)	(0.035)			(1.14)	(0.94)	(0.27)
Rh (model)	3.80	65.49	2200 ± 50	0.034	0.043	15.1%	8.5%	1.26	0.86	0.53
Rh (expt.)			(2236)	(0.034)	(0.050)			(1.57)	(0.71)	(0.72)
Ag (model)	4.09	33.72	1100 ± 30	0.034	0.043	15.1%	8.5%	1.26	0.86	0.53
Ag (expt.)			(1235)	(0.037)	(0.039)			(1.21)	(0.90)	(0.47)

[a] a_0 is the cubic lattice constant and is equal to $\sqrt{2}$ times the nearest-neighbour distance, a_{nn}.

expected to fit all properties accurately; however, because they have few parameters it may be easier to understand trends and the underlying physics of various processes. They are also longer-ranged than most 'glue' or 'embedded atom' potentials and are therefore more appropriate for describing interactions between newly fractured surfaces.

In the calculations described in this paper two Sutton–Chen potentials were used: the (10, 8) potential, which is suitable for platinum and gold, and the (12, 6) potential, which describes silver and rhodium. The sums in the potentials were computed out to 2.1 times the nearest-neighbour distance, i.e. between the fourth and fifth nearest neighbours. Note that this is slightly shorter than the cutoff used by Todd and Lynden-Bell [13]. Table 1 shows some of the properties of these metals scaled to the experimental binding energy U_0 and lattice constant a_0. Experimental numbers are given for comparison. Further properties were given in the original paper by Sutton and Chen [12] and by Todd and Lynden-Bell [13]. Of the properties that are of particular relevance to this work, the elastic constants C_{11} and C_{12} are reasonably well fit, particularly for silver and gold. An important deficiency is that the surface energies are too low†. The melting temperatures of platinum and gold are also too low, and this is correlated with the fact that the enthalpy of the (10, 8) liquid and hence the latent heat of fusion (ΔH_{fus}) are low. The main differences between the (10, 8) and (12, 6) metals are the much lower uniaxial ($C_{11} - C_{12}$) and shear (C_{44}) elastic constants and the greater relaxation found in the former metals compared with the latter.

2.2. *Method of calculation*

The calculations described in this paper were carried out using the Monte Carlo method. The system was set up in an FCC lattice with a block of $(4 \times 4 \times 4)$ unit cells ($N = 256$ particles) with periodic boundaries in the x, y and z directions. Particle positions were expressed in coordinates (s_x, s_y, s_z) scaled to the periodically repeated molecular dynamics box. The true separation between a pair of particles is given by

$$r_{ij} = a_0[n_x h_{xx}(s_{xi} - s_{xj})\hat{x} + n_y h_{yy}(s_{yi} - s_{yj})\hat{y} + n_z h_{zz}(s_{zi} - s_{zj})\hat{z}] \qquad (5)$$

where a_0 is the zero-temperature lattice constant and n_x, n_y and n_z are the numbers of crystallographic unit cells in the x, y and z directions of the simulation box; h_{xx}, h_{yy} and h_{zz} are scaling parameters and $\hat{x}$, $\hat{y}$, $\hat{z}$ are unit vectors in the corresponding cartesian directions. The initial values of the scaling parameters h_{xx}^0, h_{yy}^0 and h_{zz}^0 were taken to be

† The values for the surface energies for gold and silver in [13] have been incorrectly converted. The correct values for the (100) surfaces are 0.61 J m^{-3} for gold and 0.86 J m^{-3} for silver.

Table 2. Details of runs.

Metal	$T/[T_m]$	$10^3kT/[U_0]$	T [K]	$h^0_{xx} = h^0_{zz}$
Pt/Au	0.04	0.74	50 (Pt)	1.0007
Pt/Au	0.35	7.4	500 (Pt)	1.009
Pt/Au	0.55	11.1	750 (Pt)	1.013
Pt/Au	0.70	14.7	1000 (Pt)	1.019
Rh/Ag	0.04	1.15	75 (Rh)	1.002
Rh/Ag	0.35	11.5	750 (Rh)	1.010
Rh/Ag	0.55	18.3	1200 (Rh)	1.017
Rh/Ag	0.70	22.9	1500 (Rh)	1.023

equal to each other and chosen to give zero stress at the temperature concerned (see table 2 for values).

After equilibration, a steadily increasing uniaxial stress was applied in the (100) direction by increasing h_{xx} by a small amount at the end of each Monte Carlo cycle (in one Monte Carlo cycle, N attempted particle moves are made). In these experiments h_{yy} and h_{zz} were kept constant so that the crystal was stretched along the (100) direction with no lateral relaxation. This is in contrast with earlier experiments [10] on platinum, in which we allowed lateral relaxation. One can imagine that in the current experiments we are modelling a small portion of material embedded in a much larger crystal.

In order to compare different materials one wishes to use comparable temperatures. There are several ways of choosing the 'same' temperature for different materials; for example, one could use the same value of kT/U_0, where U_0 is the cohesive energy. Here we have chosen a different standard for setting the temperature scale, and have expressed temperatures as fractions of the melting temperature T_m of the metal concerned.

All the results were expressed as functions of the strain

$$\epsilon_{xx} = h_{xx}/h^0_{xx} - 1 \tag{6}$$

which is a dimensionless quantity. The strains ϵ_{yy} and ϵ_{zz} were both equal to zero.

Runs were carried out at four temperatures for the (10, 8) and (12, 6) potentials. Details of the temperatures and potentials are given in table 2. Before each run the sample was equilibrated and then the strain was changed at a rate of 0.1 in 20×10^3 Monte Carlo cycles. Every 200 cycles the potential energy per atom, the longitudinal and lateral stresses, and the bond order parameters Q_4, Q_6, W_4 and W_6 were stored. Configurations were written to a file for subsequent viewing every 5000 steps, i.e. at intervals of 0.025 in the strain. In most cases runs were continued to a maximum strain of 0.4.

The stress tensor is given by

$$\sigma_{\alpha\beta} = V^{-1}\left(\delta_{\alpha\beta}NkT + \sum_{\text{pairs}}(F_{ij})_\alpha (r_{ij})_\beta\right) \tag{7}$$

where $(F_{ij})_\alpha$ is the α component of the pair force (equation (4)) between atoms i and j separated by r_{ij} and V is the current volume of the sample:

$$V = n_x n_y n_z a_0^3 h_{xx} h_{yy} h_{zz}. \tag{8}$$

The orientational bond order parameters Q_L, W_L are rotationally invariant combinations of spherical harmonic functions of the vectors between neighbouring atoms [14]. We

investigated the four parameters, Q_4, Q_6, W_4 and W_6 previously used for bulk systems [15, 16]. In order to construct these, 'bonds' are drawn between all atoms nearer than a prescribed cutoff distance (equal in this work to 1.24 times the nearest-neighbour separation). The Q_L order parameters are made up of the square of sums of spherical harmonics for all N_b bonds in the sample:

$$Q_L^2 = \frac{4\pi}{N_b^2(2L+1)} \sum_m \left| \sum_{\text{bonds}} Y_{L,m}(\hat{r}_{ij}) \right|^2 \tag{9}$$

and are invariant under rotations, while the W_L functions are the third-order invariants

$$W_L = \sum_{m_1,m_2} \begin{pmatrix} L & L & L \\ -m_1 & -m_2 & m_1+m_2 \end{pmatrix} \bar{Q}_{L,-m_1} \bar{Q}_{L,-m_2} \bar{Q}_{L,m_1+m_2} \tag{10}$$

where

$$\bar{Q}_{L,m} = \frac{\sum_{\text{bonds}} Y_{L,m}(\hat{r}_{ij})}{\left(\sum_m |\sum_{\text{bonds}} Y_{L,m}(\hat{r}_{ij})|^2\right)^{1/2}}. \tag{11}$$

Two of these bond order parameters, W_4 and Q_6, proved to be particularly useful in this investigation. The important properties for the present purposes are that Q_6 is always positive and has values of about 0.5 for ideal FCC, HCP and BCC crystals. Although Q_6 would be zero for an infinite liquid, the observed values in simulations of liquids with 128 atoms and periodic boundaries were approximately 0.07 for liquid platinum/gold and silver/rhodium [16]. W_4 on the other hand can be positive or negative. The value of W_4 for simulated liquids is close to zero, while different ordered structures can be distinguished by the sign of W_4; for example, the values for ideal FCC and HCP lattices are -0.159 and $+0.134$ respectively.

2.3. *Free energy calculations*

The Landau free energy, $F(Q, T)$, is the free energy of the system as a function of some order parameter, Q. The value of F for $Q = Q_0$ can be defined by

$$\exp[-F(Q_0, T)/kT] = \int \exp(-E/kT)\delta(Q - Q_0)\mathrm{d}\tau \tag{12}$$

where the integral is over all phase space. It can be written in terms of the probability $p_Q(Q)\mathrm{d}Q$ of finding the system with a value of the order parameter between Q and $Q+\mathrm{d}Q$ as

$$F(Q) = A - kT \ln p_Q(Q) \tag{13}$$

where A is the Helmholtz free energy of the system.

The most straightforward way of determining $F(Q)$ would be to sample the canonical distribution function at the appropriate temperature and use the resulting probabilities, $p_Q(Q)$, to construct $F(Q)$. A more efficient way is to bias the system [15, 16] using a Q-dependent potential in such a way as to lower the free energy barrier. The probability $p_w(Q_0)$ of finding the biased system with the value of $Q = Q_0$ in the presence of the additional potential $w(Q)$ is then

$$p_w(Q_0) = \int \exp\left[-\left(E + w(Q)\right)/kT\right]\delta(Q - Q_0)\mathrm{d}\tau/Z(w) \tag{14}$$

where

$$Z(w) = \int \exp[-(E + w(Q))/kT]\mathrm{d}\tau \tag{15}$$

and hence

$$F(Q_0) = w(Q_0) - kT \ln p_w(Q_0) + \text{constant.} \tag{16}$$

Equation (15) allows the Landau free energy $F(Q)$ of the unbiased system to be determined. Details of the method are given elsewhere [15, 16]. Umbrella sampling, in which small ranges of the appropriate order parameters are explored separately in a Monte Carlo program with biasing potentials, was used to investigate free energy barriers for changes in the order of both metals in stretched configurations. W_4 was chosen as the order parameter because it distinguishes both between ordered and disordered states of platinum/gold and between states with different types of order in rhodium/silver. Some of the free energy calculations were carried out on a sample of 128 atoms with truncated octahedral boundary conditions to suppress void formation and fracture.

3. Initial failure

The results will be discussed separately for the regime leading from the crystal to failure and for the regime in which the crystal is stretched further. Because of the periodic boundary conditions and the comparatively small size of the system these two regimes correspond to different physical situations in real materials. The first regime corresponds to the failure of the crystal. After failure the model system rapidly forms a bridge between two new crystal surfaces so the post-failure behaviour of the model system is comparable to the stretching and breaking of a thin tongue of material between two separating surfaces.

3.1. Initial failure: platinum/gold

Figure 1 shows the variation of potential energy and longitudinal stress with strain for this material at four different temperatures $0.04T_m$, $0.35T_m$, $0.55T_m$ and $0.7T_m$, where T_m is the bulk melting temperature of the material. In each diagram the lower curve shows the stress–strain relation and the upper curve shows the potential energy as a function of strain. At finite temperatures the equilibrium stress (defined so that a negative value corresponds to a tension) is equal to minus the derivative of the free energy with respect to strain. It contains an entropic contribution in addition to the derivative of the potential energy:

$$\sigma_{\alpha\beta} = \frac{-1}{V}\left(\frac{\partial A}{\partial \epsilon_{\alpha\beta}}\right)_T = \frac{-1}{V}\left(\frac{\partial U}{\partial \epsilon_{\alpha\beta}}\right)_T + \frac{T}{V}\left(\frac{\partial S}{\partial \epsilon_{\alpha\beta}}\right)_T \tag{17}$$

where A is the Helmholtz free energy and U is the potential energy of the system. At least until failure, we shall see that the degree of disorder increases with strain, making the stress somewhat less negative than one would predict from the derivative of the potential energy curves. However, after failure the material does not behave in a reversible fashion and we cannot apply these arguments.

The stress–strain curves at different temperatures show some similar features. Initially the stretching obeys Hooke's law with the stress being a linear function of the strain, but the curves soon bend over and, except for the lowest temperature, reach a broad maximum.

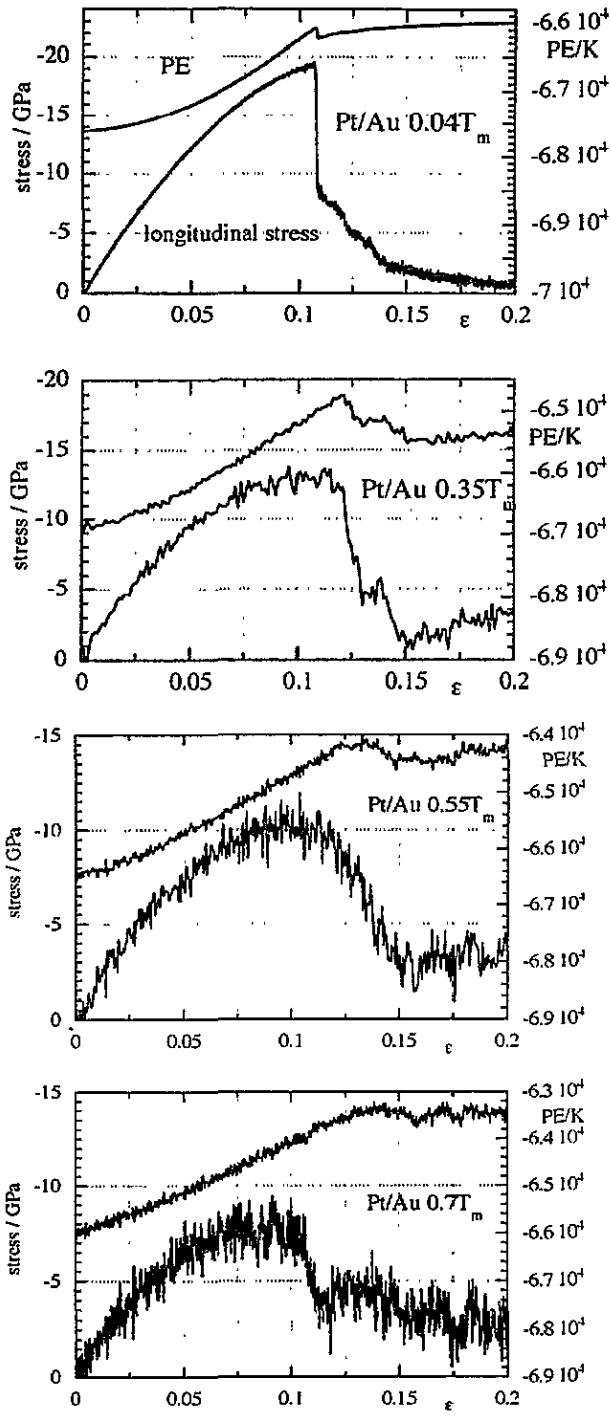

Figure 1. Longitudinal stress and potential energy as a function of strain for platinum at four temperatures. The results for gold scale; to find the stress for gold multiply the platinum stress by 0.57 and to find the potential energy multiply the platinum potential energy by 0.65. In each figure the upper curve shows the potential energy and the lower curve the stress.

This is followed by a decrease in the magnitude of the stress when the material has failed. There is rather little change in the value of the strain corresponding to maximum stress: it is about 0.1. The magnitude of the maximum stress, however, falls significantly as the temperature rises, as does the elastic constant c_{11} (which is determined by the initial slope

of the curve). The position of maximum stress is the point of failure of the material and marks the change from reversible to irreversible behaviour. The other change to be noted is that the stress falls sharply after failure at the lowest temperature, while it changes more gradually at higher temperatures. One must recall that the crystal is constrained to remain tetragonal in these experiments, and the crystal cannot elongate by processes in which the cell symmetry changes (for example, a monoclinic distortion). Values of the elastic constants C_{11} and C_{12}, and the maximum stress for platinum and rhodium, are given in table 3. To scale these values (in GPa) to the those appropriate for gold and silver respectively, one must multiply them by the ratio of U_0/a_0^3 for the two materials. Thus the values for gold are 0.57 of those for platinum, and those for silver are 0.41 for rhodium.

Table 3. Results from the simulations of platinum and rhodium.

Metal	T [T_m]	Maximum stress [GPa]	C_{11} [GPa]	C_{12} [GPa]
Pt[a]	0.0	26	315	255
Pt	0.04	19 ± 0.5	310 ± 10	250 ± 10
Pt	0.35	14.2 ± 0.2	260 ± 20	200 ± 20
Pt	0.55	10.5 ± 0.3	230 ± 20	215 ± 20
Pt	0.70	8 ± 0.5	165 ± 50	108 ± 50
Rh[a]	0.0	28.7	343	230
Rh	0.04	24.5	320 ± 10	215 ± 20
Rh	0.35	16.5	275 ± 20	175 ± 20
Rh	0.55	12.5	290 ± 20	180 ± 20
Rh	0.70	9.5	85 ± 30	60 ± 30

[a] The stresses and elastic constants for gold can be found by multiplying the values for platinum by 0.57; those for silver can be found by multiplying the values for rhodium by 0.41.

The potential energy curves increase to a maximum value and then drop. The potential energy decreases when a void is formed in the sample. This is an irreversible process which leads to fracture into two crystals. Initially the two new crystals are joined by a tongue of material, which is stretched and finally breaks as the sample is elongated. At least at the two higher temperatures, the maximum potential energy occurs at a larger strain than the maximum in the stress, showing that void formation occurs after, rather than at, the point of failure.

In order to find more information about what is happening in the material, we first look at the behaviour of the order parameters and then inspect some individual configurations. Figure 2 shows the changes in the values of the bond order parameters Q_6 and W_4 as the material is stretched at the four temperatures. Here we see a big difference between the two lower temperatures, where the order parameters decrease during failure and then recover (see the two upper graphs in the figure), and the two higher temperatures, where Q_6 and $|W_4|$ decrease to liquid-like values during failure and do not recover (see the two lower graphs in the figure).

Figure 3 shows snapshots from the platinum/gold simulations at all four temperatures. In each of these figures the direction in which the crystal is strained (x) is plotted horizontally and the small circles show the positions of the centres of the 256 atoms in the simulation cell plus some of their periodic images projected along the y direction. As the projection is along rows of atoms in the crystal many of the atoms are obscured at the lowest temperature. The cell is surrounded by periodic images on all sides. To clarify the picture we show slightly more than one periodic image of the simulation cell in the x direction. We notice that

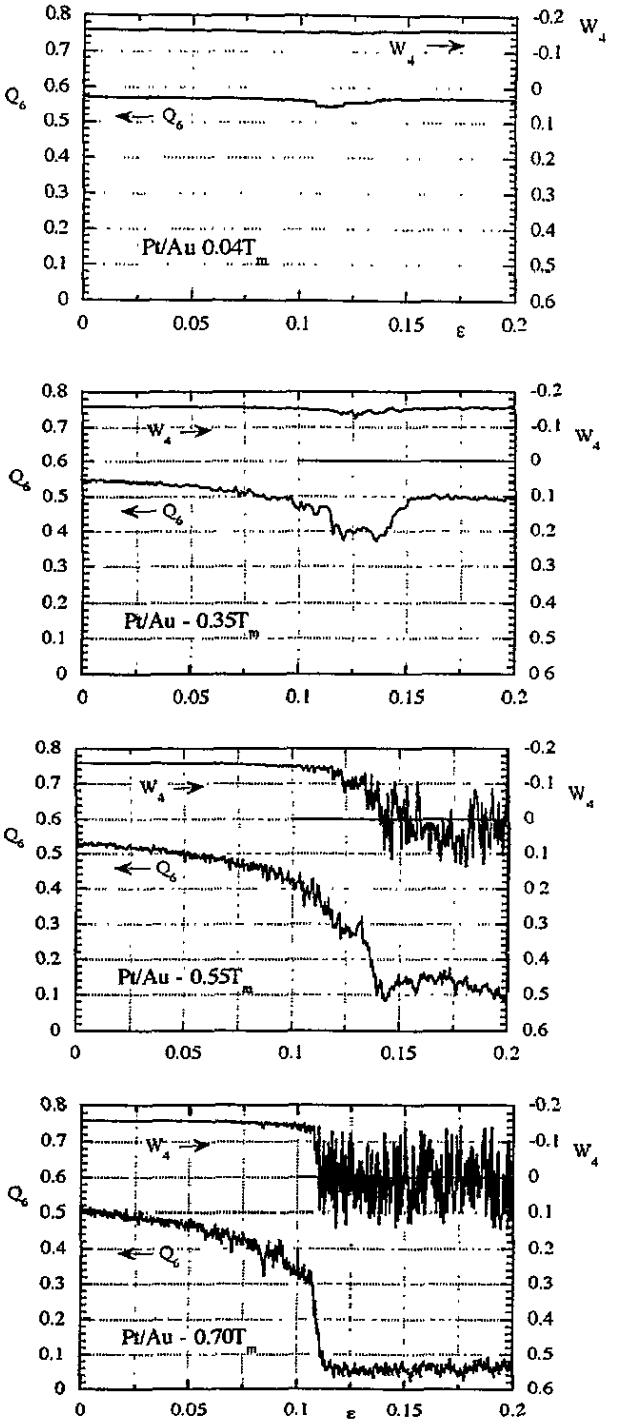

Figure 2. Values of two bond order parameters (Q_6 and W_4) as a function of strain for the same runs as in figure 1.

in every case the crystal lattice is still perfect, i.e. free from disorder or defects, in the first configuration in each sequence. These correspond to points near the maxima in the stress–strain curves, i.e. near the failure point. At larger strains we see differences. At

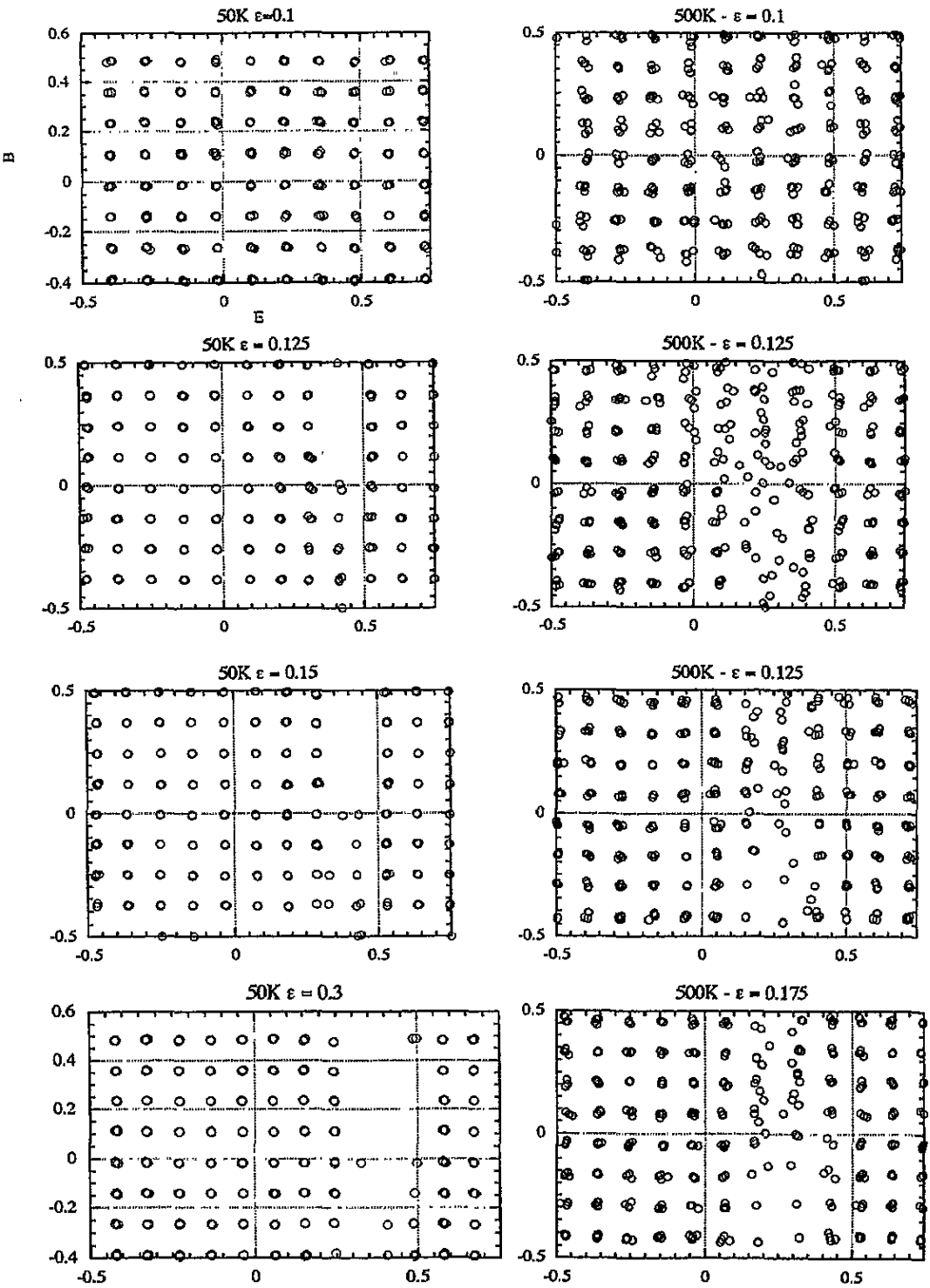

Figure 3. Configurations from the four runs for platinum shown in figures 1 and 2. (*a*) $T = 50\,\mathrm{K} = 0.04T_\mathrm{m}$. (*b*) $T = 500\,\mathrm{K} = 0.35T_\mathrm{m}$. (*c*) $T = 750\,\mathrm{K} = 0.55T_\mathrm{m}$. (*d*) $T = 1000\,\mathrm{K} = 0.7T_\mathrm{m}$.

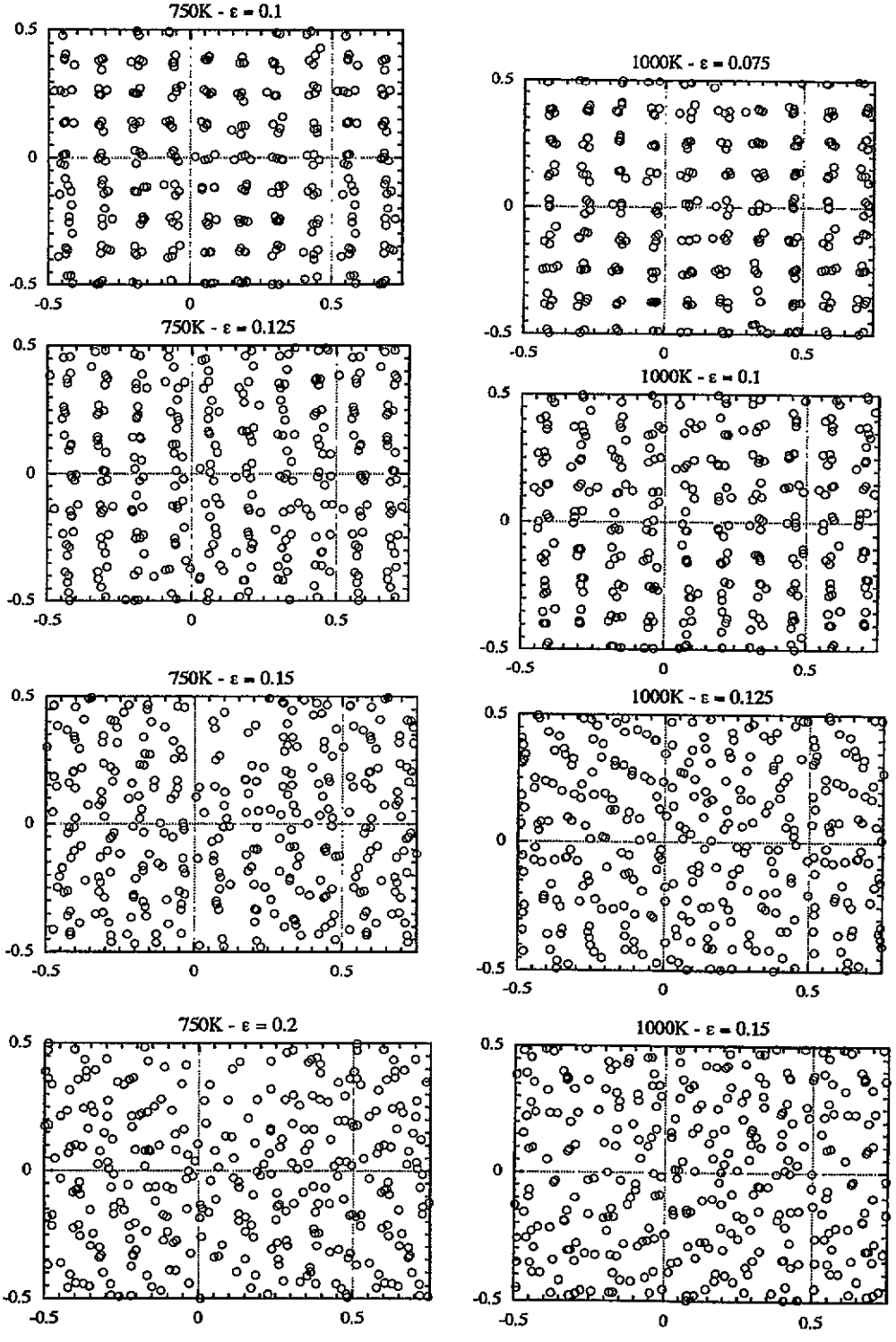

Figure 3. (Continued)

the lowest temperature ($0.04T_m$) the crystal breaks fairly cleanly leaving a few atoms in overlayers. At the next temperature ($0.35T_m$) we see a region of local disorder at a strain of 0.125 in which a void appears (see the configuration at a strain $\epsilon = 0.15$). Comparing this to the stress–strain curve in figure 1, one sees that the onset of disorder marks the point of failure. At the two higher temperatures the whole of the sample becomes disordered before the voids are formed. Evidence that the disorder occurs before the voids appear is provided by comparing the positions of the maxima in the potential energy curves with the point at which the stress begins to drop. The maxima in the potential energy curves, which mark the point of void formation, occur at progressively larger strains as the temperature increases and, particularly at the two higher temperatures, are at significantly larger strains than the point of maximum stress. This can be interpreted as showing that at least the initial decrease in stress is due to the initiation of a region of disorder, which does not greatly affect the value of the potential energy and if anything tends to increase this value, while the subsequent void formation leads to an increase in the average separation of the atoms and hence to a decrease in the potential energy.

To summarize, these results for platinum/gold show a clean break at very low temperatures, local melting at intermediate temperatures and melting of the complete sample at higher temperatures. The maximum strength is determined by the point at which disorder sets in; void formation follows at larger stresses.

3.2. Initial failure: rhodium/silver

Figures 4 and 5 show the stress–strain, potential energy–strain and order parameter–strain curves for rhodium/silver at four temperatures which correspond to the four temperatures in the platinum/gold runs. As mentioned above, they are the same proportion of the melting temperature, but a somewhat higher proportion of the binding energy.

The low-temperature curve differs from the corresponding curve for platinum/gold. Instead of there being a smooth growth in the magnitude of the longitudinal stress until failure, two dips are seen at strains of approximately 0.11 and 0.14 and, as a result, the point of failure occurs at larger stresses than for platinum/gold. The lateral stress (shown as a dotted curve) increases monotonically and becomes approximately equal to the longitudinal stress after the second dip. The order parameters change significantly at each dip, showing that each dip is associated with a structural rearrangement. Examination of individual configurations shows that layers of atoms perpendicular to the direction of pull remain well defined, but with the positions of some atoms within each layer having changed due to the fact that some (111) planes of atoms have slipped sideways. As before, when the crystal finally breaks the potential energy drops and the stresses become smaller in magnitude. Note that although the longitudinal stress drops to zero at a slightly larger strain than is shown in the figure, the lateral stress remains equal to about -10 GPa. This is due to the surface stress (surface tension) of the two new surfaces.

At the three higher temperatures the stress–strain curves are more flat-topped than those for platinum/gold, with a suggestion of a dip at $\epsilon \approx 0.125$. This is due to the formation of defects similar to those seen in the lowest-temperature run. When runs at $0.04T_m$ and $0.35T_m$ were repeated, the stress–strain curves were found to be very similar to those for previous runs at the same temperatures, with small variations in the exact values of the strain at which the dips occur and changes in the details of the resulting atomic positions. Unlike the platinum/gold simulations there is no evidence for local melting at $T = 0.35T_m$. At the two higher temperatures the samples do disorder, and here we see similarities to the platinum/gold situation. At $T = 0.55T_m$ disorder occurs and is immediately followed by void initiation and fracture, while at $T = 0.70T_m$ the sample melts at $\epsilon = 0.15$ although

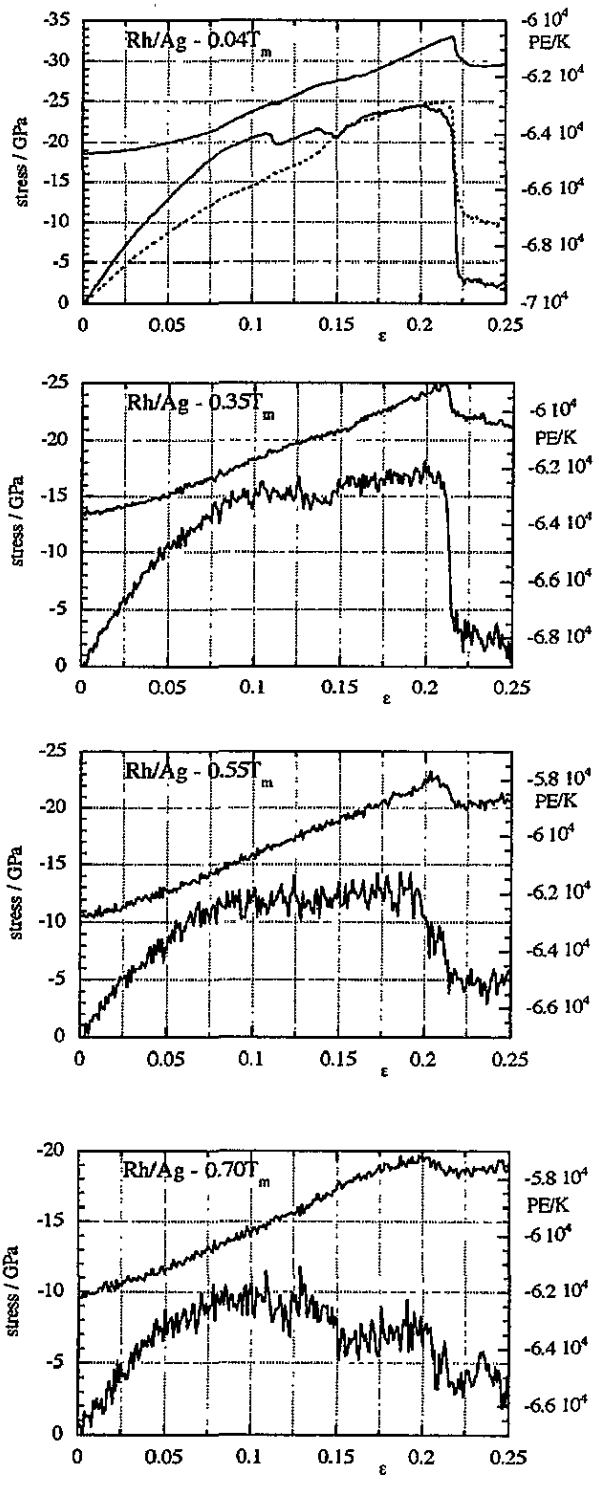

Figure 4. Longitudinal stress and potential energy as a function of strain for rhodium at four temperatures. The results for silver scale; to find the stress multiply by 0.41. and to find the potential energy multiply by 0.52. In each figure the upper curve shows the potential energy and the lower curve the stress.

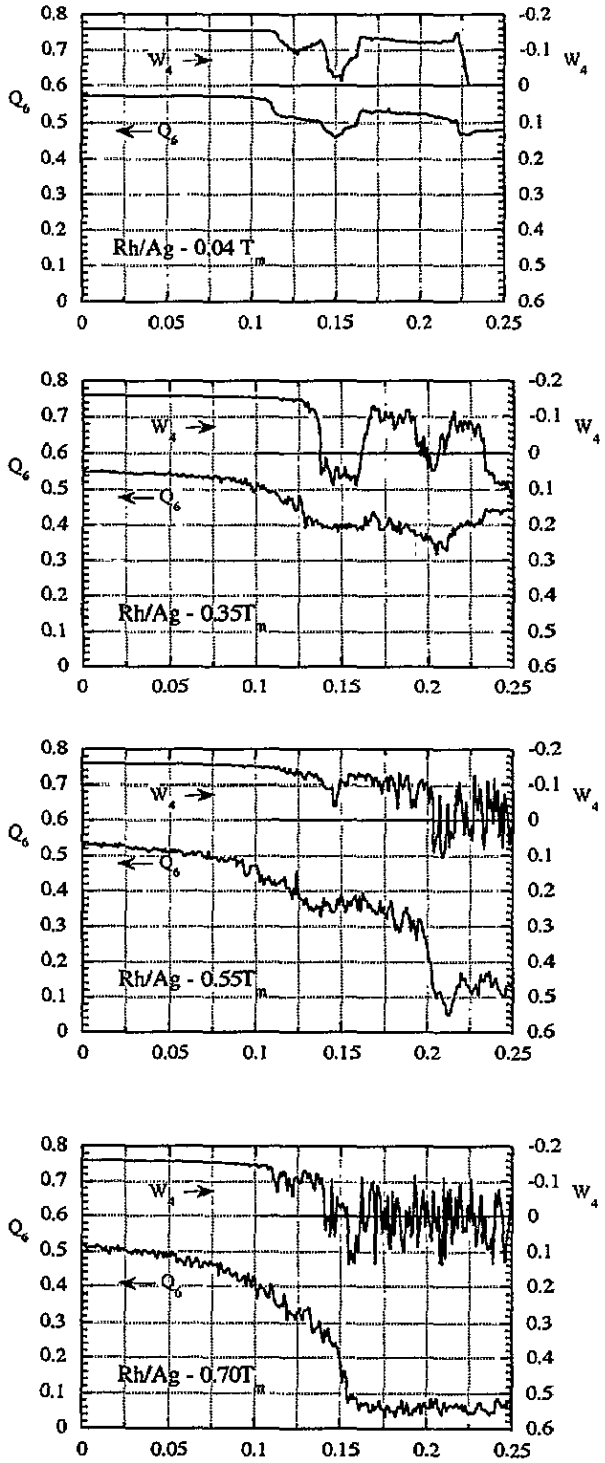

Figure 5. Values of two bond order parameters (Q_6 and W_4) as a function of strain for the same runs as in figure 4.

void formation does not occur until it is stretched to $\epsilon = 0.2$. The point of failure at these temperatures is associated with the onset of disorder.

The order parameter curves (figure 5) also show what is happening when the sample changes structure. At both $T = 0.35T_m$ and $0.55T_m$ the values of Q_6 decrease somewhat, while W_4 fluctuates from negative to positive values when this happens. The changes in structure are again the result of lateral displacements of (111) planes of atoms perpendicular to the direction of strain.

To summarize, for the rhodium/silver sample, the formation of defects allows the crystal to stretch further before failure than the platinum/gold sample. At $T = 0.55T_m$ the final failure occurs via melting and void formation, as for the platinum/gold material at the corresponding temperature. There are, however, no signs of local disorder before failure of rhodium/silver at $T = 0.35T_m$. At $T = 0.70T_m$, the sample melts at $\epsilon \approx 0.15$, but void formation is postponed until $\epsilon \approx 0.20$.

4. Free energy considerations

An infinite stretched crystal is always metastable with respect to two separate crystals with new interfaces as the surface free energy of the new interfaces is negligible compared with the bulk free energy. In a system with periodic boundaries, such as we have in these numerical experiments, the surface free energy of the new interfaces cannot be neglected. Nevertheless the ordered crystal becomes metastable at a small value of the strain, ϵ. Figure 6 shows the free energies of various possible states of the system schematically. The curve marked X refers to the ordered crystalline form, that marked X2 refers to separated crystals with two new surfaces and the curve marked D refers to the disordered form. As the strain on the system is increased the free energy follows curve X. Although the stretched crystal becomes metastable when this curve crosses the curve X2, there is a high free energy barrier to fracture (i.e. to curve X2), as it is difficult to initiate a void in an ordered crystal. For the platinum/gold crystal we postulate that the sample continues to follow the curve X until it crosses the curve D, which is the disordered curve. The free energy barrier to the order/disorder change is smaller than that to fracture. After the system crosses from curve X to curve D and disorders it can reach equilibrium following the vertical path shown with an arrow, because once it is disordered it is comparatively easy for a void to be formed and the sample to break.

This scenario is consistent with the numerical experiments for platinum at the two highest temperatures, where we observe that the system disorders and then a void appears. At the lower temperature ($T = 0.35T_m$), only a portion of the crystal was observed to disorder. This can also be explained using figure 6. The curve D shifts downwards as the temperature is lowered. If we draw a common tangent to the curves X and D, we see that the system can lower its free energy by dividing into two portions, one ordered and one disordered, the former having a smaller strain and the latter a larger strain, keeping the same average strain. One may conjecture that the region of disorder in a very large sample would be larger, but finite, at higher temperatures, but exceeds the size of our simulation box at the two higher temperatures.

In order to pursue these ideas further, I investigated the variation of the Landau free energy with order parameter for platinum/gold at $T = 0.55T_m$ at three values of the strain, $\epsilon = 0.1$, 0.125 and 0.135 which, as can be seen from figure 1, correspond respectively to (i) the point of maximum stress (failure), (ii) a configuration with a higher potential energy but less stress, and (iii) the point of maximum potential energy. The resulting Landau free

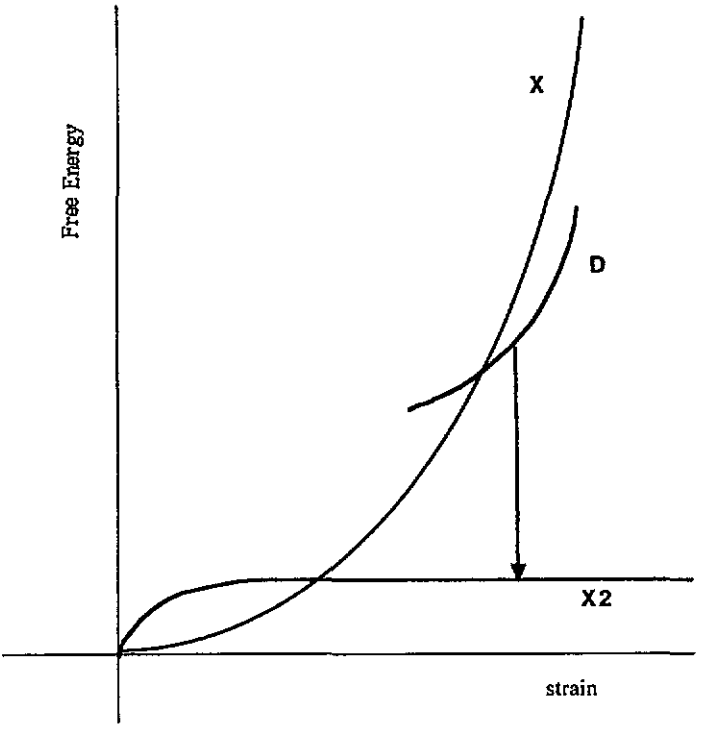

Figure 6. Schematic free energies of different possible states of a stretched crystal as a function of strain. States are marked as follows. X: a single perfect crystal; X2: two perfect crystals; D: disordered liquid-like state.

energy curves as a function of Q_6 are shown in figure 7. The minimum corresponding to the ordered state (i.e. the curve marked X on figure 6) is on the right of these figures; the corresponding value of Q_6 decreases with strain as expected from the Q_6 versus strain curves in figure 2. The second minimum associated with the disordered state (D on figure 6) does not exist at $\epsilon = 0.1$ (where the stress is a maximum). As the strain is increased this minimum deepens until it becomes equal to the ordered state minimum at $\epsilon \approx 0.135$. This must correspond to the point on figure 6 where the curves D and X cross. The free energy barrier to the change from order to disorder is only about twice kT. Careful examination of the order parameter against strain curves in figure 2 shows that the change from order to disorder occurs at about this strain. This confirms that the sample follows the free energy path in figure 6 along X, and across to D. The free energy curves were constructed with truncated octahedral boundary conditions to suppress nucleation of voids. In the sample in the strain experiments void formation soon follows disorder.

4.1. Rhodium/silver

The difference between the platinum/gold and rhodium/silver samples is most apparent at the lower temperature of $0.35T_m$. Between $\epsilon \approx 0.135$ and the breaking point, the sample fluctuates between positive and negative values of W_4 before settling down to a positive value. As we have seen this region is one where defects are formed as planes of atoms slide sideways past each other. In order to investigate the free energies involved, Landau free energy curves were again constructed, but this time with cubic boundary conditions.

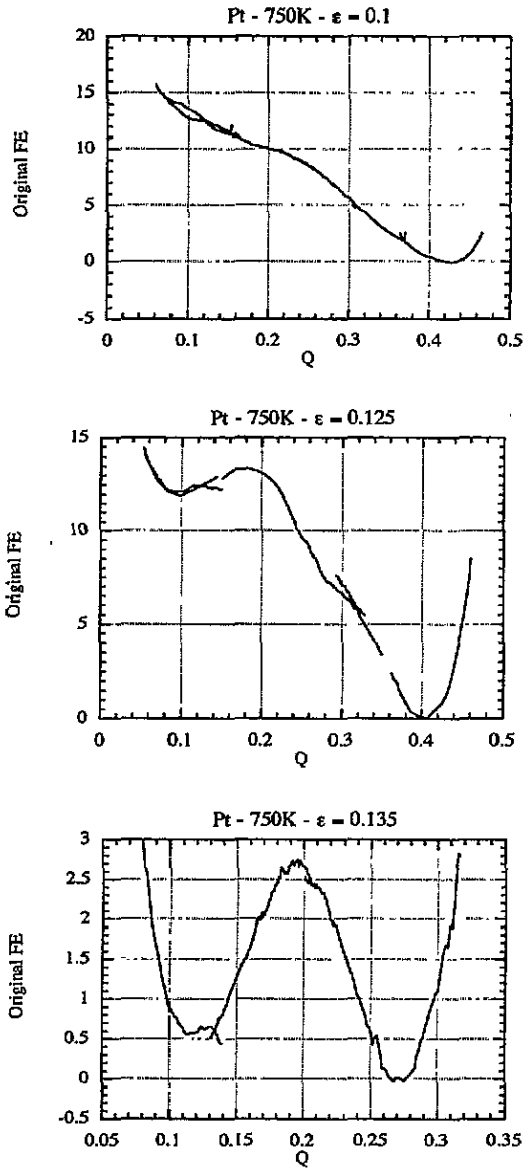

Figure 7. Landau free energy as a function of the order parameter Q_6 for platinum at 750 K ($0.55T_m$) at three different strains. The left-hand well corresponds to the disordered state (D in figure 6) and the right-hand well to the perfect crystal (X in figure 6).

The curves are shown in figure 8 for a strain of $\epsilon = 0.15$ using the order parameter W_4. Two different starting configurations were chosen to generate the two curves shown. The change is from the stretched FCC ordered phase with a negative value of W_4 (the left-hand minimum) to two different phases with slipped planes (the right-hand minima). The two points to notice are firstly that the free energy barriers are small and secondly that there is no minimum at $W_4 = 0$ that would correspond to a disordered phase. This confirms that the sample has a number of nearby free energy minima corresponding to various ways in which the planes of atoms can slip, and either has no minimum corresponding to a disordered state or such a minimum is inaccessible.

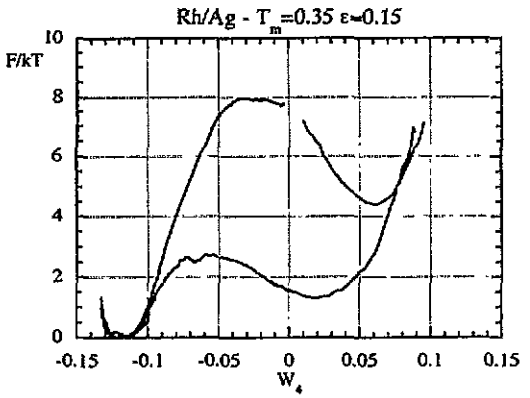

Figure 8. Landau free energy as a function of the order parameter W_4 for rhodium/silver at $0.35T_m$. The left-hand well corresponds to the perfect crystal and the right-hand wells to two possible states with defects. Note that there is no indication of a disordered state at $W_4 = 0$.

4.2. Origin of differences

The macroscopic properties of materials formed using the platinum/gold and the rhodium/silver potential have some distinct differences, some of which are shown in table 1. The most striking of these is the ratio of the shear elastic constant to the bulk compressibility, which changes from 0.26 for platinum/gold to 0.53 for rhodium/silver [12]. This can be attributed in part to the softer potential of the former material, although more detailed analysis shows that it is the difference in the exponents n and m that is the most important factor [13]. Another marked difference is in the melting points of the two materials. The melting point of platinum/gold is 2.1% of the cohesive energy, while that of rhodium/silver is 3.3%. This difference is mainly due to the difference in heats of fusion of the two model materials, that for rhodium/silver being about 1.5 times as large as that for platinum/gold. The other factor that could influence the propensity for the stretched crystal to disorder is the change in volume on melting. This is about 7.8% for platinum/gold and 8.5% for rhodium/silver.

These differences in bulk properties are reflected in differences in microscopic properties. For example [13, 17] the amount of relaxation either at the surface of the metal, around an adatom or around a vacancy is much greater in Sutton–Chen potentials with small differences in the exponents. The most striking result of this is that the mechanism of migration of adatoms is by exchange with surface atoms in the case of platinum/gold, while such a mechanism has a very unfavourable activation energy for silver/rhodium [17].

The differences observed in the current numerical experiments can be related to these properties, the question being whether the free energy of accessible defective states is lower than that of accessible disordered states or not. The final step in the failure of each sample is the formation of a void. Although this is particularly favoured by the low surface energies of the platinum/gold potential, these numerical experiments indicate that the crucial step is the surmounting of the free energy barrier to void formation. This barrier is very high in the perfect crystal and comparatively low in disordered material, so that the formation of a disordered region provides a route to failure. This is what we observed in platinum/gold. The mechanism of failure in the rhodium/silver material is different at low temperatures, and this is manifest even at the very lowest temperature used where, in contrast to the platinum/gold material, dislocations form spontaneously as the material is stretched. This allows the material to sustain a greater strain before failure. It seems likely that the reason that the platinum/gold tends to disorder rather than form dislocations is that the free energy of the disordered state is lower than in rhodium/silver, so that disorder occurs in preference to dislocations under the constraints of these experiments. We know that at zero stress the

disordered state has a lower free energy (in reduced units) in platinum/gold compared to rhodium/silver as the melting temperature is so much lower. It is not surprising then that this is true under conditions of finite stress.

We should note that if the temperatures are compared as a function of the binding energy the difference between platinum/gold and rhodium/silver is larger (see table 2). For example, the temperature at which complete disorder occurs in the rhodium sample is considerably higher than in platinum sample, although they have comparable lattice energies.

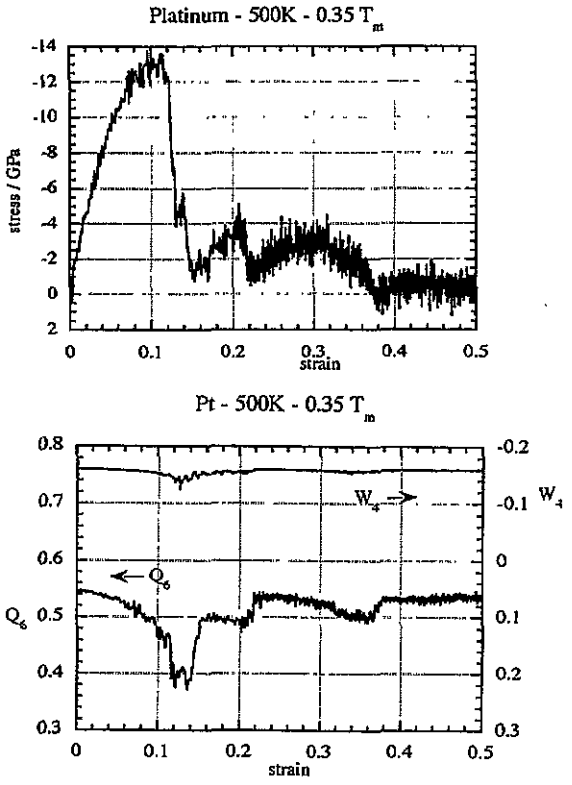

Figure 9. The variation of stress and order parameters as a function of strain for platinum at $0.35T_m$ in the post-failure regime.

5. Bridge stretching and breaking: platinum/gold

Because of the periodic boundary conditions, the void that is formed initially soon becomes a bridge. The way in which a bridge behaves when stretched is of interest, as a thin whisker of material is formed when an atomic or scanning tunnelling microscope tip comes into contact with a flat [2]. Recent experiments by Agraït and co-workers [3] show steps in the conductivity as this bridge is stretched. In the numerical experiments described in this paper the bridge formed is much smaller than those seen in Agraït's experiments, but at lower temperatures one does see some steps in the stress–strain curves after failure. Similar steps were found in earlier work on rhodium/silver [9] and with Lennard-Jones potentials [8]. In the current experiments on platinum/gold at the two higher temperatures, $0.7T_m$ and $0.55T_m$, there is no structure in the stress–strain curves after the initial failure, but at $0.35T_m$ two

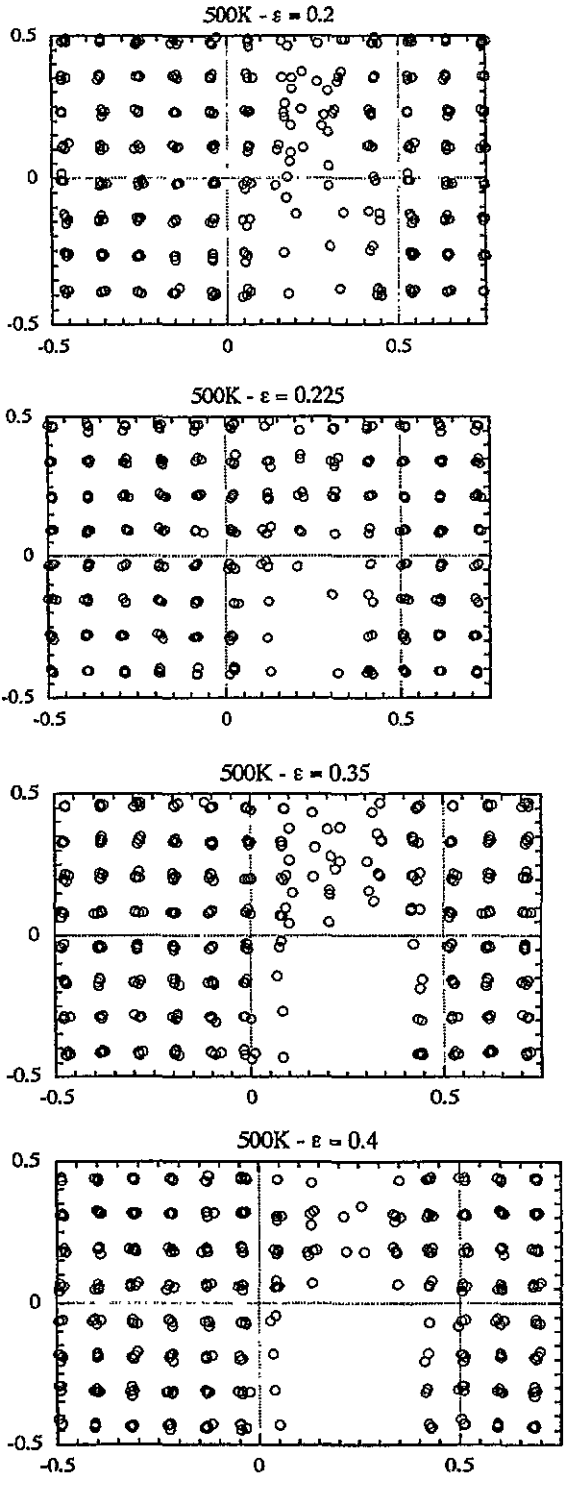

Figure 10. Four configurations from the run in figure 9 showing that the changes in stress and Q_6 correspond to transitions to states in which the order in the bridge has increased.

secondary steps are seen in figure 9, one at $\epsilon \approx 0.21$ and the other at $\epsilon \approx 0.37$. After each step the stress and potential energy both increase. The sequence of configurations in figure 10 shows clearly what is happening. The bridge formed at this temperature is initially crystalline, but as it is stretched it becomes more disordered, and the magnitude of the stress and potential energy increase until a structural change occurs. As a result the atoms assume a new ordered configuration with an extra layer, reducing both the stress and the potential energy. The upper two configurations in the figure are just before and just after the first such structural change. This process is then repeated, and the lower two configurations are before and after the second change. If the bridge were longer, then one would expect more such steps in the stress–strain curve. At the higher temperatures, on the other hand, the bridge is completely disordered and so stretches uniformly rather than in jerks.

6. Discussion and conclusions

These results are of interest for two reasons: firstly as giving insights into the way that real materials may fail under some experimental conditions, and secondly as a study of the limits of stability and mechanism of failure of perfect crystals when stretched.

These numerical experiments suggest that if a perfect crystal of platinum or gold were stretched along the (100) direction failure would be brought about by thermal fluctuations which caused a small region of disorder. This relieves the strain locally and will tend to grow as a lens shaped volume with a concentration of stress at its edges. The higher the temperature the larger this volume would become before void formation occurred, followed by fracture. In rhodium and silver there are competing processes, which are particularly important at low temperatures.

The results show that melting, or at least disordering, occurs well below the zero-pressure thermodynamic melting point in both platinum/gold and rhodium/silver when the crystals are uniaxially stretched. This is consistent with what one would expect from the Clausius–Clapeyron equation for the change is melting point with pressure

$$\left(\frac{\mathrm{d}T}{\mathrm{d}p}\right)_{\mathrm{coex}} = \frac{\Delta V}{\Delta S}. \tag{18}$$

However, the sample is certainly not in thermodynamic equilibrium (or it would break into two crystals) and it is not immediately clear whether this equation is applicable.

A perfect crystalline phase has limits of metastability outside which it cannot exist. For example, when the temperature is raised eventually the free energy minimum corresponding to the crystalline phase disappears [16]. This limit of stability (or metastability) has been termed the mechanical melting temperature by Yip and co-workers [18, 19]. It can be thought of as the point at which the amplitude of vibrations of the atoms in the crystal becomes great enough that the lattice breaks down. Similarly, there are limits of metastability for stretched crystals. These have been investigated at zero temperature for a number of systems [20, 21], and the question is whether the observed failure of the crystals in these experiments is at the limits of metastability of the stretched crystals.

The free energy calculations for the platinum/gold model show that this is not true. What we are observing in the stretching experiments at the higher temperatures is the point at which the free energy of the ordered and disordered phases become equal, rather than the limit of stability of the phase. The evidence for this is that the Landau free energy curves show two minima, one for the ordered and one for the disordered phase. The free

energy barrier between the two phases is low enough that it can be surmounted by thermal fluctuations, so failure occurs at the thermodynamic melting temperature of the stretched metastable crystal into the stretched metastable liquid.

At lower temperatures both model materials undergo other changes on the way to reaching the true thermal equilibrium state of separate crystals, either local disorder or defect formation.

In all these experiments the strain rather than the stress is constrained so that the observed phase transitions are under conditions of constant strain rather than constant stress. This is akin to observing a transition in an isotropic system at constant density rather than under the more usual conditions of constant pressure. However, the effects of the periodic boundary conditions are important here. At constant strain a sufficiently large system could lower its free energy by separating into regions of the two different phases with the same overall density. Indeed, we saw this behaviour in the platinum sample at the lower temperature ($T = 0.35T_m$), although the periodic boundaries make separation more difficult. A larger sample might be expected to phase separate at higher temperatures, where our sample was completely disordered.

Acknowledgments

I should like to thank J van Duijneveldt for the use of his program which has been adapted for this work, and SERC for computational support through grants GR/H/04190 and GR/K/20651.

References

[1] Macmillan N H and Kelly A 1986 *Strong Solids* (Oxford: Clarendon)
[2] Kuipers L and Frenken J W M 1993 *Phys. Rev. Lett.* **70** 3907
[3] Agraït I 1994 *Phys. Rev. Lett.* **1** 1
[4] Parrinello M and Rahman A 1980 *Phys. Rev. Lett.* **45** 1196
[5] Wang Z-G, Landman U, Selinger R L B and Gelbart W M 1991 *Phys. Rev.* B **44** 378
[6] Lupkowzki M and Maguire J F 1992 *Phys. Rev.* B **45** 13733
[7] Blonski S, Brostow W and Kubát J 1994 *Phys. Rev.* B **49** 6494
[8] Lynden-Bell R M 1992 *J. Phys.: Condens. Matter* **4** 2127
[9] Lynden-Bell R M 1994 *Science* **263** 1704
[10] Selinger R L B, Lynden-Bell R M and Gelbart W M 1993 *J. Chem. Phys.* **98** 9808
[11] Finnis M W and Sinclair J E 1984 *Phil. Mag.* A **50** 45
[12] Sutton A P and Chen J 1990 *Phil. Mag. Lett.* **61** 139
[13] Todd B D and Lynden-Bell R M 1993 *Surface Sci.* **281** 191
[14] Steinhardt P J, Nelson D R and Ronchetti M 1983 *Phys. Rev.* B **281** 784
[15] van Duijneveldt J and Frenkel D 1992 *J. Chem. Phys.* **96** 4655
[16] Lynden-Bell R M, van Duijneveldt J and Frenkel D 1993 *Mol. Phys.* **4** 801
[17] Lynden-Bell R M 1991 *Surface Sci.* **259** 129
[18] Phillpot S R, and Lutsko J F, Wolf D and Yip S 1989 *Phys. Rev.* B **40** 2831
[19] Lutsko J F, Wolf D, Phillpot S R and Yip S 1989 *Phys. Rev.* B **40** 2841
[20] Zwicky F 1923 *Z.Phys.* **24** 131
[21] Macmillan N H and Kelly A 1972 *Proc. R. Soc.* A **330** 291